Wire ablation dynamics model and its application to imploding wire arrays of different geometries

A. A. Esaulov, V. L. Kantsyrev, A. S. Safronova, A. L. Velikovich, I. K. Shrestha, K. M. Williamson, and G. C. Osborne

Phys. Rev. E **86**, 046404 — Published 22 October 2012

DOI: 10.1103/PhysRevE.86.046404

Wire Ablation Dynamics Model and its application to imploding wire arrays of different geometries

A. A. Esaulov[1], V. L. Kantsyrev[1], A. S. Safronova[1], A. L. Velikovich[2],
I. K. Shestha[1], K. M. Williamson[1,3], and G. C. Osborne[1]
[1]*Department of Physics, University of Nevada, Reno, Nevada 89557, USA*
[2]*Plasma Physics Division, Naval Research Laboratory, Washington, D.C. 20375, USA and*
[3]*Sandia National Laboratories, Albuquerque, NM 87185, USA*

The paper presents an extended description of the amplified Wire Ablation Dynamics Model (WADM) that accounts in a single simulation for the processes of the wire ablation and implosion of a wire array load of arbitrary geometry and wire material composition. To investigate the role of the wire ablation effects, the implosions of cylindrical and planar wire array loads at the university based generators Cobra (Cornell University) and Zebra (University of Nevada, Reno) have been analyzed. The analysis of the experimental data shows that the wire mass ablation rate can be described as a function of the current through the wire and some coefficient defined by the wire material properties. The aluminum wires were found to ablate with the highest rate, while the copper ablation is the slowest one. The lower wire ablation rate results in higher inward velocity of the ablated plasma, higher rate of the energy coupling with the ablated plasma, and more significant delay of implosion for a heavy load due to the ablation effects, which manifest the most in a cylindrical array configuration and almost vanish in a single planar array configuration. The WADM is an efficient tool suited for wire array load design and optimization in wide parameter ranges, including the loads with specific properties needed for the Inertial Confinement Fusion research and laboratory astrophysics experiments. The data output from the WADM simulation can be used to simplify the radiation MHD modeling of the wire array plasma.

PACS numbers: 52.59.Qy, 52.58.Lq

I. INTRODUCTION

For more than a decade the physics of wire array loads imploded by ≥ 1 MA currents attracts a significant attention in scientific community, mainly because of the high conversion ratio of the stored electromagnetic energy into the soft and hard x-ray radiation achieved with these loads. The most energetic and powerful x-ray source is created at the Sandia National Laboratories (SNL) where single and nested cylindrical wire array loads are imploded at 26 MA Z accelerator producing the record high > 2 MJ radiation energy yield and > 280 TW radiation power [1, 2] relevant to the Inertial Confinement Fusion (ICF) research [3, 4].

Despite these remarkable achievements the search for new, more effective wire array load configurations continues [5]. This search has inspired several extensive programs for studying the wire array implosion at 1 MA currents at the university based laboratories, first at the Imperial College in UK [6, 7] and later at the University of Nevada, Reno (UNR) [8–11] and Cornell University (see, for example, Ref. [12]) in the United States. Smaller environment of a typical university laboratory allows much lesser cost of each wire array shot and relatively high number of these shots per one experimental campaign.

In 2005 a novel wire array configuration, a planar wire array, was tested as the x-ray radiation source at 1 MA Zebra facility at UNR [8]. Since that time numerous experiments have demonstrated that among all the other low-wire-number loads the planar wire arrays yield the highest x-ray radiation energies and powers [9–11]. Two years later, the single planar array loads have been successfully tested at $3-5$ MA currents on Saturn generator at SNL [5, 13, 14]. By now, several novel applications of planar wire arrays have been proposed and tested at UNR, such as the new hohlraum design for ICF-related experiments [5], the possibility of controlling the shape of the x-ray radiation pulse [15], the experiments with multi-planar arrays related to the laboratory astrophysics [16], and skewed wire double planar array configurations with induced axial magnetic field [17]. A continuous success in these research directions can be assured by the development and application of reliable modeling tools.

While the magnetohydrodynamic (MHD) codes remain the most adequate tools that can be applied for simulation of hot and dense wire array plasmas, some intrinsic features of a wire array configuration require these codes to account for two spatial scales that differs by three orders of their magnitudes: a typical load size of tens of mm and a typical wire size of tens of μm. Then, a typical MHD simulation takes a few days on a computer cluster. At the same time, any model simplifications, which intend to increase computational speed, seriously impede the predictive capabilities of these simulations (see, for example, the discussions in Refs. [18–21]).

Generalization of the ideas set forth in Ref. [22] resulted in the development of an efficient alternative simulation tool for wire array loads of arbitrary geometry, the Wire Dynamics Model (WDM) [18, 19] that takes less than one minute simulation time on average personal computer. The WDM has been successfully applied to model the nested cylindrical [12] and single- and multi-planar [19] wire arrays in the current range from 1 MA university level generators to $3-5$ MA current levels at SNL [5, 13, 14]. Nevertheless, despite an obvi-

ous efficiency of the WDM, its dynamic picture of imploding wire arrays is quite limited mainly because the momentum redistribution to the plasma ablated from the array wires is disregarded, which among other issues leads to an inaccurate prediction of the implosion time for some heavy wire array loads [12]. Consideration of the dynamics of ablated plasma is also critical for numerous important applications of wire array physics, such as, for example, the x-ray radiation pulse shaping and the laboratory astrophysics experiments.

An upgrade of the original WDM to the Wire Ablation Dynamics Model (WADM), introduced in Ref. [23], has been performed on principle of adding thin current filaments to describe the momentum redistribution to plasmas ablated from the array wires. Later this approach has been justified by the successful application of the WADM to the simulation of single and nested cylindrical arrays [24] and single- and double-planar arrays [11, 25, 26].

This paper introduces the comprehensive description of the amplified WADM with its enhanced features, including the detailed discussion on determination of the ablation rate coefficients from the analysis of the experimental data. The effects due to the variation of the ablation rate coefficients for different wire materials are discussed on the example of cylindrical wire arrays. The applications of the enhanced features of the WADM, such as the estimation of the kinetic energy thermalization rate and calculating the structure and some parameters (mass and current densities) of the ablated plasma flows, are discussed on the example of planar wire arrays. The general features of the ablation and implosion dynamics of Al wire arrays are compared for the cylindrical, single- and double-planar geometries. The conclusive remarks are given in the last chapter of this paper.

II. MODEL DESCRIPTION

The Wire Ablation Dynamics Model is an upgrade of the original Wire Dynamics Model [18, 19] and uses the same equation of motion of thin filaments carrying some currents. The key difference between these two models is that the WADM allows momentum redistribution between the ablating array wires and the ablated plasmas.

A. Dynamics of current filaments

The acceleration of the kth current filament ($k = 1, 2, \ldots, K$) on the complex plane (x, y) is defined by the following equation:

$$\frac{d^2\xi_k}{dt^2} = \frac{F_k}{\mu_k} \ , \tag{1}$$

where $\xi_k = x_k + iy_k$ is the complex coordinate and μ_k is the mass per unit length of the kth filament. The complex variable $F_k = F_{kx} + iF_{ky}$ represents the components of the Lorentz force on kth filament, induced by all other current filaments and the return currents

$$F_k = -\frac{\mu_0}{2\pi} I_k \sum_{\substack{l=1 \\ l\neq k}}^{K} I_l \left[\frac{\xi_k - \xi_l}{|\xi_k - \xi_l|^2} - \frac{a^2\xi_l - |\xi_l|^2\xi_k}{|a^2 - \xi_k\bar{\xi}_l|^2} \right] \ . \tag{2}$$

In the above equation I_k is the electric current through the kth filament, and the bar sign denotes a complex conjugate value. This equation for the Lorentz force (2) represents the most general case of a wire array in a cylindrical return current can of the radius a, where the return currents are reduced to an image filament with negative current [the second term in parenthesis in the right-hand side of Eq. (2)].

As it was discussed in Ref. [19], the model of the inductive current partition through the array wires recreates the most adequate physical picture, which is in closest agreement with the experimental data. According to this model, the current partition through the filaments can be found as a solution of the system of K linear equations

$$I_k \ln \frac{a^2 - |\xi_k|^2}{ar_f} + \sum_{\substack{l=1 \\ l\neq k}}^{K} I_l \ln \frac{\left|a^2 - \xi_k\bar{\xi}_l\right|}{a\left|\xi_k - \xi_l\right|} = \frac{2\pi\Lambda}{\mu_0} \ , \tag{3}$$

where r_f is the effective filament radius, and Λ is the value of the magnetic flux per unit length contributed from the self inductance and mutual inductance of the filaments. The approximation of thin wires [18, 19, 22] requires

$$r_f \ll \min_{l\neq k} \left\{ \left|a - \xi_l\right|, \left|\xi_k - \xi_l\right| \right\} \ . \tag{4}$$

In Eq. (3) Λ is actually the $(K+1)$th unknown variable in the system of K equations, which has to be completed by adding the current normalization equation

$$\sum_{k=1}^{K} I_k = I \ , \tag{5}$$

where I is the total current through the wire array load. Now, the load inductance L can be defined from the following relation [19, 22])

$$l_z\Lambda = LI \ , \tag{6}$$

where l_z is the length of the wire array load (or the distance between the electrodes).

B. Mass and momentum redistribution

In the WDM each array wire is represented by a single current filament. In that case the parameter K in Eqs. (2)–(5) is equal to the number of array wires N. Associating multiple current filaments with a single array wire, the WADM can simulate the plasma ablation from the array wires and the momentum transfer to the streams of the ablated plasma directed toward the array center. In the latter case new current filaments carry current and momentum of the ablated plasma.

Below in this paper the array wires will be denoted by the index $n = 1, 2, \ldots, N$, while each wire will be represented by a single current filament. The ablation process is modeled by splitting this current filament into two new filaments. One of these filaments will still represent the nth array wire that continues to ablate, while another filament will represent the ablated plasma and will be allowed to move freely in the collective magnetic field of the wire array. The production of new filament is performed at the same time for each array wire in sequence of the moments t_j separated by the same time intervals Δt

$$t_j = j \cdot \Delta t \ , \quad j = 1, 2, \ldots, J \ . \tag{7}$$

For the convenience of filament identification the second index "j" will be introduced. The filament with subscript $n0$ ($j = 0$) will represent the nth ablating array wire. The filament denoted by the double subscript nj ($j \geq 1$) will represent the ablated plasma filament produced by the nth wire at $t = t_j$ [Eq. (7)]. Now, in the equations (1)–(2) defining the filament dynamics in a self-consistent magnetic field of the array and in the equations (3)–(5) defining the current partitions through filaments the summation over the single index k should now be replaced with the summation over the double index nj so that $K = N \times J$. In order to account for mass and momentum transfer from the array wires to the ablated plasma, some special conditions will be imposed separately on the filaments having indexes $n0$ (array wires) and nj with $j \geq 1$ (ablated plasma filaments).

We assume the mass ablation rate per unit wire length

$$\frac{d\mu_{n0}}{dt} = -G_n \left[I_{n0}\right]^{\alpha} \ , \tag{8}$$

where μ_{n0} is the wire mass per unit length, I_{n0} is the electric current through the nth wire, and G_n is the constant wire ablation rate coefficient.

So far the WADM simulations of various cylindrical and planar low wire number ($N \leq 24$) array configurations with $\alpha = 2$ in Eq. (8) at $1-1.7$ MA currents have revealed quite a good agreement with the experimental data (see, for example, Refs. [23–26]). The value $\alpha = 2$ in Eq. (8) suggests the wire ablation rate to be proportional to the power deposition due to the Ohmic heating $R_\Omega [I_{n0}]^2$, where R_Ω is the electric resistance of the wire. In the meantime, for the cylindrical arrays with higher wire number the lower values of the parameter α have been suggested: $\alpha = 1.8$ for the intermediate wire number $N = 60 - 80$ cylindrical array loads at 3 MA current level [27, 28], and $\alpha = 1.4 - 1.55$ for the high wire number $N = 200 - 300$ cylindrical wire array loads at 20 MA current level [20, 21].

For each array wire the WADM assumes a stepwise decrease of mass per unit length after each moment of current filament splitting

$$\mu_{n0}(t) = \begin{cases} \mu_{n0}(0) & , \ 0 \leq t < t_1 \\ \mu_{n0}(0) - \sum\limits_{m=1}^{j} \mu_{nm} & , \ t_j \leq t < t_{j+1} \end{cases} \ , \tag{9}$$

where $\mu_{n0}(0)$ is the initial mass per unit length of the nth array wire, and the specific mass μ_{nj} of newly produced current filaments ($j \geq 1$) is defined according to Eq. (8) as

$$\mu_{nj} = G_n \int\limits_{t_{j-1}}^{t_j} \left[I_{n0}(t)\right]^{\alpha} dt \ . \tag{10}$$

Eqs. (9)–(10) describe the mass transfer from the array wires to the ablated plasma, while the total mass of all filaments stay constant all the time.

With the rise of the electric current, the mass of the ablated plasma filaments increases according to Eq. (10), while the wire mass constantly decreases in time [Eq. (9)]. The special WADM algorithm ensures that the specific mass the wire $\mu_{n0}(t_*)$ remaining after splitting is still larger that the specific mass μ_{nj} of the newly produced ablated plasma filament. The correspondent condition

$$\mu_{n0}(t_*) \geq 2G_n \int\limits_{t_{j-1}}^{t_j} \left[I_{n0}(t)\right]^{\alpha} dt \ , \quad t_{j-1} \leq t_* < t_j \tag{11}$$

is checked before the filament splitting at $t = t_j$ the ensure the consistency of Eq. (9).

If the condition (11) can not be fulfilled, then no filament splitting for nth array wire will be performed after t_{j-1}, and the ablation of the nth wire will be completed at $t = t_a^{(n)}$, where $t_{j-1} < t_a^{(n)} < t_j$. The ablation time for nth wire $t_a^{(n)}$ can be found as a solution of the implicit equation

$$\mu_{n0}\left(t_a^{(n)}\right) = 2G_n \int\limits_{t_{j-1}}^{t_a^{(n)}} \left[I_{n0}(t)\right]^{\alpha} dt \ , \tag{12}$$

which is performed numerically in the WADM simulation.

From the time of the first experiments with cylindrical wire arrays imploded at university scale 1 MA machines it was found that the array wires do not move until their ablation is complete [6, 7]. Later, the same features of implosion dynamics of the cylindrical wire arrays has been observed at 20 MA current level [29, 30]. Full momentum transfer from the array wire to the ablated plasma can be explained by strong radial gradients of density in the heterogeneous core-corona structure (also, see the above references). At such conditions a low-density plasma of wire corona is much easier to be accelerated than a heavy wire core. Eventually, as the wire ablation completes, the radial gradients of density substantially diminish, momentum transfer decreases, and the wire start to move as a single object.

In the WADM wires do not move until their ablation is complete

$$\frac{d\xi_{n0}}{dt} = u_{n0}(t) = 0 \quad \text{for} \quad t < t_a^{(n)} \ , \tag{13}$$

while the momentum $\int F_{n0} dt$ accumulated for the period $t_{j-1} < t < t_j$ ($t_j < t_a^{(n)}$) is transferred to the ablated plasma

filament produced at $t = t_j$

$$\left.\frac{d\xi_{nj}}{dt}\right|_{t=t_j} = u_{nj}(t_j) = \frac{1}{\mu_{nj}} \int\limits_{t_{j-1}}^{t_j} F_{n0}(t)dt \ . \qquad (14)$$

After the ablation of nth array wire is complete at $t = t_a^{(n)}$ (assuming $t_{j-1} \le t_a^{(n)} < t_j$), this array wire becomes an ablated plasma filament, having all the mass

$$\mu_{nj} = \mu_{n0}(t > t_{j-1}) \qquad (15)$$

and momentum

$$u_{nj} = \frac{1}{\mu_{nj}} \int\limits_{t_{j-1}}^{t_a^{(n)}} F_{n0}(t)dt \qquad (16)$$

of the remains of the nth wire. As the condition (13) is no longer applicable, this filament allows to move freely in the collective magnetic field of the imploding array.

In a simulation of the wire array ablation and implosion the trajectories of ablated plasma filaments eventually may cross. When the critical proximity $r_\delta = C_\delta r_f$ between two filaments is reached, these filaments merge into a single filament (inelastic collision), which has the combined mass and momentum of the two filaments before merging. The deficient amount of the kinetic energy ΔW_{Th} is recorded as an increase of the internal energy of plasma. Summation over these step-wise increments ΔW_{Th} provide the evolution of total thermalized kinetic energy $W_{Th}(t)$.

The critical proximity of filaments in the center of the array r_p is typically larger than r_δ in order to adequately account for the diameter of precursor plasma column, imposing the restriction $r_p > C_\delta r_f$. It should be noted here that the parameter r_p remains constant during the simulation. Hence, the same value will represent the effective radius of the resultant z-pinch, which is known to define the final value of thermalized kinetic energy (see, for example, the discussion in Ref. [31]). In accordance with experimental data in the most simulations the effective precursor/pinch radius is taken as $r_p = 150 - 250$ μm. Respectively, the typical values of the critical proximity factor and the filament radius in the simulations are $C_\delta = 5$ and $r_f = 20 - 30$ μm.

The ablated plasma filaments are produced near their "parent" wires (placed at ξ_{n0}) with the positions ξ_{nj} slightly shifted toward the array center

$$\xi_{nj} = \xi_{n0} \cdot \left[1 - \frac{C_a r_f}{|\xi_{n0}|}\right] \ , \ j \ge 1 \ . \qquad (17)$$

The factor $C_a > C_\delta$ in the above equation regulate the distance between array wire and the newly produced filament. For obvious reasons the condition $C_a > C_\delta$ should be satisfied, while the recommended value in the simulations is $C_a = C_\delta + 1$.

To perform the simulation the geometry, mass and size of the wire array load is input into the code, which calculates the initial masses μ_{n0} and positions ξ_{n0} of the wires. The shape of the current pulse is extracted from the experimental data. The wire ablation rate coefficients G are input into the code as the values, which were determined earlier for each specific wire material. For a uniform load a single ablation rate coefficient G is applied. If a wire array load is composed of two or more wire materials, then each material is assigned a specific ablation rate coefficient.

C. Additional features of the WADM

The WADM simulation provides the information about the filament mass and the current through the filament during the array ablation and implosion. However, in numerous applications the information about the continuous spatial distribution of plasma mass density and current density is more valuable than the discrete data calculated by the WADM.

A quasi-continuous two-dimensional distributions of mass density $\rho(x, y)$ and current density $j_z(x, y)$ on the complex plane can be reconstructed from the WADM output data. This routine can be performed if we assume the Gaussian-like distributions of the mass and current densities with the centers at the position of the ablated plasma filament ξ_{nj} having the specific mass μ_{nj} and carrying current I_{nj}

$$\rho^{(nj)} = \rho_0^{(nj)} e^{-(r/a)^2} \text{ and } j_z^{(nj)} = j_0^{(nj)} e^{-(r/a)^2} \ , \qquad (18)$$

where r is a distance to the observation point $\xi = x + iy$: $r = |\xi_{nj} - \xi|$, a is the spatial smoothing scale, and the amplitudes

$$\rho_0^{(nj)} = \frac{\mu_{nj}}{\pi a^2} \text{ and } j_0^{(nj)} = \frac{I_{nj}}{\pi a^2} \qquad (19)$$

are chosen to conserve the mass and the magnetic flux

$$\int\limits_0^\infty \rho^{(nj)} 2\pi r dr = \mu_{nj} \text{ and } \int\limits_0^\infty j_z^{(nj)} 2\pi r dr = I_{nj} \ . \qquad (20)$$

Now, two dimensional quasi-continuous distributions of mass and current densities can be obtained after summation over all active filaments

$$\rho(x, y) = \sum_{n,j} \rho^{(nj)} \text{ and } j_z(x, y) = \sum_{n,j} j_z^{(nj)} \ . \qquad (21)$$

Another useful algorithm that can be applied to post-process the WADM data output is related to the shape of the x-ray radiation pulse. According to the WADM the thermal energy W_{Th} experiences an instant finite increase by ΔW_m after mth inelastic collision of the current filaments at the moment $t = t_m$. Thus, the correspondent thermalization rate P_m can be is expressed in the terms of a δ-function

$$P_m(t) = \Delta W_m \delta(t_m) \qquad (22)$$

normalized due to the energy conservation law as

$$\int\limits_{-\infty}^{+\infty} P_m(t)dt = \Delta W_m \ . \qquad (23)$$

Hence, the total thermalization rate P according to the WADM is some set of infinitely narrow pulses with infinite amplitude defined by the sum over all filament collisions

$$P(t) = \sum_m P_m(t) = \sum_m \Delta W_m \delta(t_m) \ . \tag{24}$$

In the WADM output the only finite parameter related to the thermalization rate P is the time-resolved increment of thermal energy

$$\Delta W_{Th}(t) = \sum_m \Delta W_m(t_m) \ . \tag{25}$$

The thermalization rate defines the power input into the plasma. As the most of this power is immediately radiated, the thermalization rate should also be able to describe the x-ray radiation pulse from the imploding load with reasonable accuracy (see, for example, the discussions in Refs. [23]). More realistic shape of the thermalization rate (finite pulse width and pulse amplitude) can be obtained, for example, in MHD simulations, which use a continuous media approximation rather than the approximation of discrete thin filaments. Consideration of the magnetic Rayleigh–Taylor (MRT) instability modes in MHD simulations also results in broadening of the calculated x-ray pulse [32, 33].

Alternatively, in the WADM the artificial function broadening of the rates P_m is applied

$$P_m^*(t) = \frac{\Delta W_m}{\sqrt{\pi} a} \exp\left(- \left[\frac{t - t_m}{a} \right]^2 \right) \ , \tag{26}$$

where constant a represents the pulse semi-width, while smoothed P_m^* pulse has the same normalization as the original P_m pulse in Eq. (23) in order to obey the energy conservation law. The summation over all collisions provides the following smoothed shapes for the total thermalization rate $P^*(t)$ and the correspondent evolution of total thermalized kinetic energy $W_{Th}^*(t)$:

$$P^*(t) = \sum_m P_m^*(t) \text{ and } \quad W_{Th}^*(t) = \int_0^t P^*(\tau) d\tau \ . \tag{27}$$

The application of these additional features will be considered in greater details in the Section IV of this paper.

III. MODELING OF CYLINDRICAL WIRE ARRAYS

In a cylindrical array geometry all wires carry the same current I/N, have the same ablation rate coefficients G, and complete their ablation at the same time t_a

$$I_{n0} = g_0 \frac{I}{N} \ , \quad G_n = G \ , \quad t_a^{(n)} = t_a \ , \tag{28}$$

where g_0 is the factor of the order of unity representing the fraction of the total electric current conducted by the array wires. The implosion trajectories $\xi_{nj}(t)$ of all wires of the cylindrical array are also identical:

$$|\xi_{nj}(t)| = r_j(t) \ , \quad j = 0, 1, 2, \ldots, J \ . \tag{29}$$

These intrinsic features related to rotational symmetry of the cylindrical wire arrays make them perfect experimental objects for observation and study of wire ablation dynamics.

A. Determination of wire ablation rate coefficients

If the wire ablation is disregarded, then the implosion of a cylindrical wire array is described by the 0D model equation

$$r \frac{d^2 r}{dt^2} = - \frac{N-1}{N} \frac{\mu_0}{4\pi} \frac{I(t)^2}{m_L} \ , \tag{30}$$

where m_L is the wire array mass per unit length. The above equation has only one characteristic time scale, the array implosion time t_{0D}: $r(t_{0D}) = 0$, which is defined by the array mass and size and is independent of the wire array material properties.

The WADM introduces the second time scale, the wire ablation time t_a, which depends on the properties of wire material through the ablation rate coefficient G: rewriting Eq. (12) we get

$$\int_0^{t_a} [I_{n0}(t)]^\alpha \, dt = \frac{\mu_{n0}(0) - \mu_{n0}(t_a)}{G} \approx \frac{\mu_{n0}(0)}{G} \ . \tag{31}$$

To compare these two different time scales it will be convenient to introduce the dimensionless parameter f_τ

$$f_\tau = \frac{t_a}{t_{0D}} \ . \tag{32}$$

Since wires do not move during the ablation period $t < t_a$, one can expect some insignificant departure of the wire implosion trajectories from the ones predicted by the 0D model (30) at $f_\tau \ll 1$. This departure, however, will be significant at $f_\tau \sim 1$.

Fig. 1 shows the results of the WADM modeling of the cylindrical wire array with mass and geometry of the load in Cobra shot No. 658: compact cylindrical Al wire array with $N = 16$, array diameter $D = 6$ mm, array mass $M = 68$ μg. Three different values of the parameter f_τ have been applied in the WADM simulations. As we can see, in the case of the prolonged wire ablation $f_\tau > 0.7$ the array implosion time t_{imp} increases with respect to the value t_{0D} predicted by 0D model. This increase can be evaluated by another dimensionless parameter f_i

$$f_i = \frac{t_{imp}}{t_{0D}} \ . \tag{33}$$

As we can see from the analysis of the simulation data shown in Fig. 1 the parameter f_i is some monotonic function of the wire ablation time t_a in the range $f_i > 1$. Thus, if

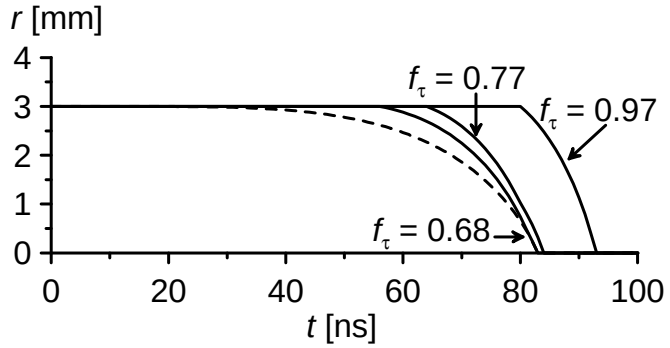

FIG. 1. WADM simulations of the cylindrical array implosion (Cobra shot No. 658). Dotted line represents the implosion trajectory in no-ablation approximation ($f_\tau = 0$). Solid lines represents the implosion trajectories in wire ablation approximation with three non-zero values of the parameter f_τ.

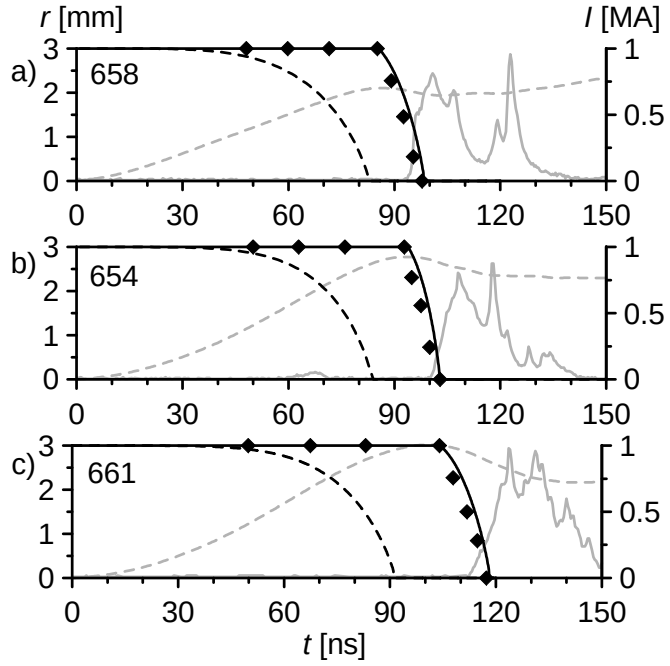

FIG. 2. WADM simulations of the implosions of compact cylindrical arrays in the Cobra shots No. (a) 658 (Al), (b) 654 (stainless steel), and (c) 661 (brass). The wire implosion trajectories in WADM simulations (black solid lines) are compared with evolutions of wire positions (black symbols) extracted from the optical streak camera images. Black dotted lines represent the wire implosion trajectories in no-ablation approximation ($f_\tau = 0$). Solid and dotted grey lines show the experimental x-ray pulse (PCD signal, arbitrary units) and current pulse shape I respectively.

we know the value f_i from the analysis of the experimental data, and if $f_i > 1$, then the ablation rate coefficient G can be unambiguously derived from the correspondent WADM simulation.

Fig. 2 presents the WADM simulation results for cylindrical wire arrays made of three different materials: Al (Cobra shot No. 658), stainless steel (Cobra shot No. 654), and brass (Cobra shot No. 661). The values of the parameter f_i for these shots were found to be different: $f_i = 1.18$, $f_i = 1.22$, and $f_i = 1.18$ respectively (in all three cases the moment of implosion corresponds to a sharp increase of the x-ray radiation pulse). Based on these vales, the wire ablation rate coefficients were found to be $G = 7$ μg/mm$\cdot$(ns^{-1}MA^{-2}) for Al wires, $G = 4.8$ μg/mm$\cdot$(ns^{-1}MA^{-2}) for stainless steel wires, and $G = 4.3$ μg/mm$\cdot$(ns^{-1}MA^{-2}) for brass wires. As we can see from the analysis of these data, the wires made of different materials ablate with different rates at the same level of the electric current.

The data in Fig. 2 show that only the calculated implosion times t_{imp} match the experimental data, but the whole implosion trajectories fairly reproduce the experimental implosion trajectories extracted from the optical streak camera images. Direct comparison of the implosion trajectories obtained in experiments and simulations is the alternative method of determination of the ablation rate coefficient in the situation, when $f_i = 1$ ($f_\tau < 0.7$).

B. Wire ablation and implosion in cylindrical array geometry

To consider the wire ablation and array implosion dynamics in a cylindrical array geometry we shall consider in greater details the Cobra shot No. 658 (Al compact cylindrical array). The differences in the implosion features between the cylindrical array loads built of different wire materials will be discussed in the next subsection.

The WADM simulation of the Cobra shot No. 658 is shown in Fig. 3. The array wires finish their ablation at $t_a = 85$ ns. Since in this simulation $\Delta t = 8$ ns, then $J = 11$ [Eq. (7)]. The last ablated plasma filament $j = J$ describes the implosion dynamics of wire remnant until the array implosion at $t_{imp} = 98$ ns. As we can see in Fig. 3(b), it takes over 20 ns from the current pulse start for the first ablated plasma filaments ($j = 1$) to reach the array center. Then, a quasi-stationary inward flow of the ablated plasma is established ($3 \le j \le 10$) until the end of implosion phase.

The analysis of the implosion trajectories in Fig. 3(b) show that $r_j(t)$ [Eq. (29)] is some monotonic function. Thus, we can redefine filament velocity u_{nj} as a function of the filament position v_j

$$\frac{d}{dt}\,|\xi_{nj}(t)| = \frac{dr_j(t)}{dt} = |u_{nj}(t)| = v_j(r_j)\ . \qquad (34)$$

Functional dependencies $v_j(r_j)$ are presented in Fig. 4(a). At early time the ablated plasma moves with higher velocity ($j = 1, 2$). Later at $t > 20$ ns, as the inner volume of the array is filling up with the ablated plasma filaments, all significant acceleration happens only in the vicinity of the array wires. Then, the ablated plasma filaments converge toward the array center practically with the constant velocity v_p

$$v_j(r_p) \approx v_p\ , \qquad (35)$$

where r_p is the assumed effective radius of the precursor

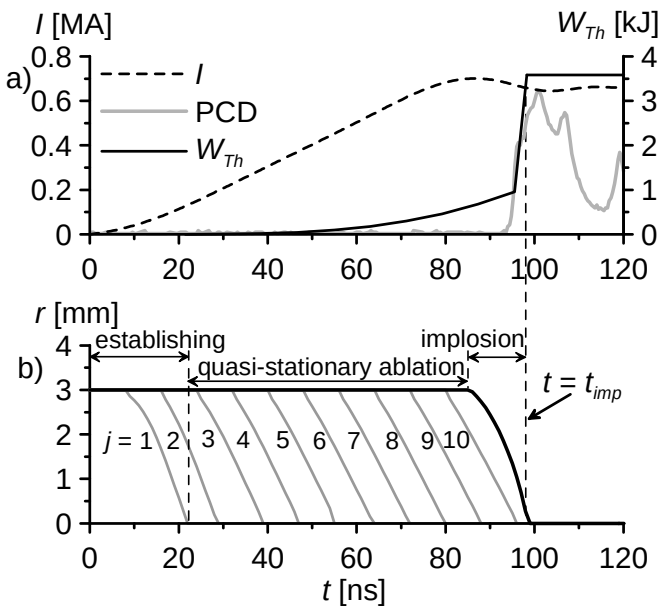

FIG. 3. Implosion dynamics of Al compact cylindrical array (Cobra shot No. 658). (a) Experimental current pulse shape I and the PCD signal (arbitrary units). Thermalized kinetic energy W_{Th} is calculated by the WADM. (b) Initial positions ($j = 0$, black line) and implosion trajectories ($j = 11$, black line) of the array wires and ablated plasma filaments ($j = 1, 2, \ldots, 10$, grey lines), calculated by the WADM.

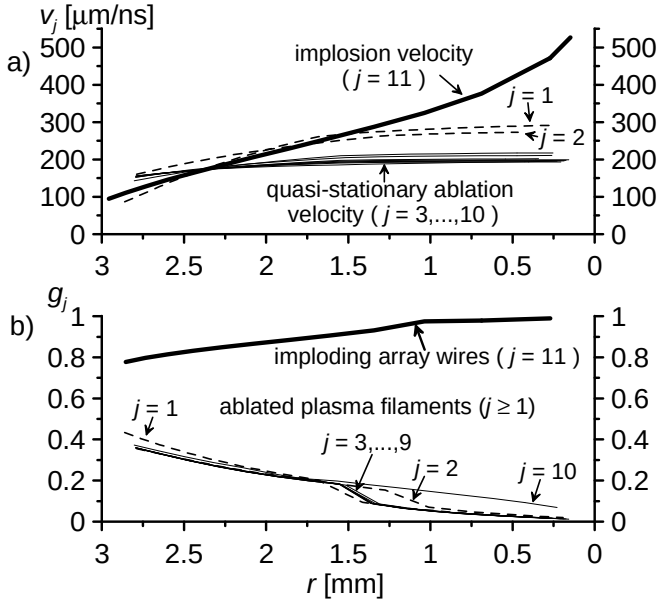

FIG. 4. WADM simulation of the Cobra shot No. 658: (a) filaments velocities v_j [Eq. (34)] and (b) normalized currents through the filaments g_j [Eq. (36)] as the functions of the filaments positions r_j.

plasma column. In the Cobra shot No. 658 this asymptotic velocity value is $v_p = 200$ μm/ns.

Such behavior can be explained by the specific partition of current through the ablated plasma filaments $I_{nj}(r_j)$. The distribution of the normalized currents g_j

$$g_j(r_j) = \frac{N}{I} I_{nj}(r_j) \tag{36}$$

is shown in Fig. 4(b). In the WADM the inductive current partition model describes screening of the electric current by the ablating array wires from the inner regions of the array. The major part of the electric current $g_0 = 60 - 80\%$ is carried by the ablating array wires. The rest of the current is carried by the newly produced ablated plasma filaments: $g_j(r_j) \sim 30 - 40\%$ at 2.5 mm$< r_j <$ 3 mm. As the ablated plasma filament moves toward the array center, the value of current through this filament rapidly decreases: $g_j(r_j) < 5\%$ at $r_j < 0.5$ mm.

Plasma mass accretion $M_p(t)$ at the center of the array is described by the formula

$$M_p(t) = l_z N \sum_{j=1}^{J_p(t)} \mu_{nj} \ , \tag{37}$$

where $J_p(t)$ is the stepwise function representing the highest index j for all filaments that have arrived to the array center and merged into a single column by the time t, so that $M_p(t \geq t_{imp}) = M$. During the merge the kinetic energy of each ablated plasma filament transforms into the thermal energy of plasma.

The total thermalized kinetic energy $W_{Th}(t)$ is

$$W_{Th}(t) = l_z N \sum_{j=1}^{J_p(t)} \frac{\mu_{nj} v_j^2(r_p)}{2} \ . \tag{38}$$

The evolution of W_{Th} in the Cobra shot No. 658 is shown in Fig. 3(a). During the ablation phase $t < t_{imp}$ we can apply the approximation (35). Thus,

$$W_{Th}(t) \approx M_p(t) \frac{v_p^2}{2} \quad (t < t_{imp}) \tag{39}$$

the increase of W_{Th} during the ablation phase is mostly due to the accretion of mass M_p at the array center.

One of the most important parameters that describe the radiation performance of plasma is the internal energy per one ion ε

$$\varepsilon(t) = A m_u \frac{W_{Th}(t)}{M_p(t)} \ , \tag{40}$$

where A is the atomic weight of the wire material and m_u is the atomic mass unit. Using the approximation (39) we can now estimate the value ε as a result of a kinetic energy thermalization

$$\varepsilon(t) \approx \varepsilon_p = A m_u \frac{v_a^2}{2} \quad (t < t_{imp}) \ . \tag{41}$$

The WADM simulation of the Cobra shot No. 658 yields $\varepsilon_p = 5.4$ keV.

In its turn, the internal energy of plasma is distributed between the thermal, ionization U and radiation E_{rad} energies

$$\varepsilon = \frac{3}{2}\left(\bar{Z}+1\right)T_p + U(\bar{Z}) + E_{rad} \ , \tag{42}$$

where $\bar{Z}$ is the mean ion charge of plasma. We can estimate the upper bound for temperature T_p^* neglecting the radiation energy in the above equation $E_{rad} = 0$

$$\varepsilon_p = \frac{3}{2}\left(\bar{Z}+1\right)T_p^* + U(\bar{Z}) \ . \tag{43}$$

For $\varepsilon_p = 5.4$ keV the ionization balance model, which and is currently implemented in the radiation MHD code POS [34] and is based on the Local Thermodynamic Equilibrium (LTE) approximation, yields $T_p^* = 190$ eV. The accurate calculation of the precursor plasma temperature can only be achieved with the radiation MHD modeling, since the key factors that defines plasma temperature, the radiation cooling and the spatial structure of plasma column (see, for example, detailed discussion in Ref. [31]), are not resolved in the WADM simulations.

After wire ablation completes, the implosion dynamics of the wire remnant is described by the motion of the ablation filament with the number $j = J = 11$. The dynamics of such filaments is quite different from the dynamics of the filaments $3 \le j \le 10$ describing the quasi-stationary ablated plasma flow because of the high value of fractional currents $g_J = 80\% - 100\%$ [see Fig. 4(b)]. As a result, the filaments $j = J$ experience increasing inward acceleration as they approach the array center

$$\frac{d^2 r_J}{dt^2} \propto -\frac{1}{r_J} \ . \tag{44}$$

As we can see from Fig. 4(a) at $r = r_p$ the filament velocity is $v_J(r_p) \approx 2.5 v_p$ [Eq. (35)] with the kinetic energy

$$W_{imp} = l_z N \frac{\mu_{nJ} v_J^2(r_p)}{2} \ . \tag{45}$$

In the Cobra shot No. 658 $\mu_{nJ} \approx 0.3\mu_{n0}(t=0)$.

For a cylindrical array W_{imp} is mostly a function of the current pulse amplitude $I_{\max}$ and the compression ratio (r_0/r_p) (see, for example, Ref. [31])

$$W_{imp} \approx 0.8 \frac{\mu_0}{4\pi} l_z I_{\max}^2 \ln\frac{r_0}{r_p} \ , \tag{46}$$

where μ_0 is the permeability of free space, and $r_0 = |\xi_{n0}|$ is the initial array radius. Hence, influence of the specific properties of wire material on the value W_{imp} is insignificant.

The increase of thermalized kinetic energy due to the term W_{imp} is the only effect considered by the 0D or the WDM models, which disregard wire ablation dynamics. The WADM additionally calculates the amount of the kinetic energy W_p thermalized during the ablation stage

$$W_p = l_z N \sum_{j=1}^{J-1} \frac{\mu_{nj} v_j^2(r_p)}{2} \ . \tag{47}$$

TABLE I. Load parameters and WADM simulation results for compact cylindrical arrays imploded at Cobra generator

Shot No.	Material	M [μg]	G $\left[\frac{\mu g\cdot(ns)^{-1}}{mm\cdot(MA)^2}\right]$	v_p $\left[\frac{\mu m}{ns}\right]$	f_i	ε_p [keV]	T_p^* [eV]	f_W
658	Al	68	7	200	1.18	5.4	190	2.8
654	stainless steel	78	4.8	290	1.22	25	250	1.7
661	brass	124	4.3	310	1.29	32	290	1.2

Contrary to the W_{imp}, the value of W_p is greatly affected by the specific properties of the wire material.

Thus, according to the WADM the final value of the thermalized kinetic energy $W_\Sigma = W_{Th}(t > t_{imp})$ is a sum of two components

$$W_\Sigma = W_p + W_{imp} \ . \tag{48}$$

The jump of the function $W_{Th}(t)$ at $t = t_{imp}$ [see Fig. 3(a)] can be evaluated by the parameter

$$f_W = \frac{W_{imp}}{W_p} \ . \tag{49}$$

In the Cobra shot No. 658 the WADM simulation yields $W_p = 0.95$ kJ, $W_\Sigma = 3.6$ kJ ($r_p = 150$ μm) and $f_W = 2.8$.

C. Effects due to the properties of wire material

In order to understand the influence of the effects due to the specific properties of wire materials on wire ablation and array implosion dynamics we shall consider below three shots with the same load geometries, but made of aluminum (Cobra shot No. 658), stainless steel (Cobra shot No. 654) and brass (Cobra shot No. 661) wires. The implosion trajectories calculated by the WADM for these shots are shown in Fig. 2, while the major simulation parameters are given in the Table I.

As we can see from the Table I, lower values of the mass ablation rate coefficient G for the stainless steel and brass wires results in higher velocities v_p of inward flow of the ablated plasmas during quasi-stationary ablation phase. A lower value of coefficient G leads to a lower mass of newly produced ablated plasma filament, while in the same array geometry the same amount of momentum is transferred to the ablated plasma filament. Thus, in the same array geometry we can expect $v_p \propto 1/G$.

The rocket model [6, 7] equation represents the differential form of the mass transfer equation (14), simplified for the cylindrical geometry

$$V\frac{dm_l}{dt} = \frac{\mu_0}{2\pi}\frac{I^2}{D} \ , \tag{50}$$

where m_l is the total ablated mass per unit length of the array, D is the array diameter and V is the ablation velocity.

Besides the momentum transfer, Eq. (50) also represents a simplified form of the mass production equation (8), where the parameter $1/V$ in the rocket model has the same meaning as coefficient G in the WADM. However, the parameters V (v_p in the WADM) can only be defined for the cylindrical array geometry. Besides, numerous simulations of wire arrays of different geometries and wire material compositions performed with pilot versions of the WADM have shown that the value of ablation rate coefficient G is only a function of wire material (at least at $1 - 1.8$ MA current levels). This justified the use of coefficient G in the final version of WADM to describe the ablation properties of the wire materials.

Also, a lower value of the mass ablation rate coefficient in the same array geometry results in longer ablation time of the wire of the same mass [Eq. (31)] on the scale of the array implosion time. Thus, for lower values of coefficient G we should expect higher values of the parameter f_i. This observation is confirmed by the data in the Table I.

Finally, a lower value of coefficient G and, consequently, higher value of the ablation velocity v_p leads to a higher value of the thermalized kinetic energy and potentially hotter plasma. Recently, a very hot 400 eV precursor plasma created by the implosion of low wire number cylindrical array has been reported in Ref. [35]. Since the value of energy coupling at the implosion phase W_{imp} is not sensitive to the specific properties of wire materials, we should expect lower energy contrast ratio f_W for the wire arrays having lower values of coefficient G. This observation is also confirmed by the data in the Table I.

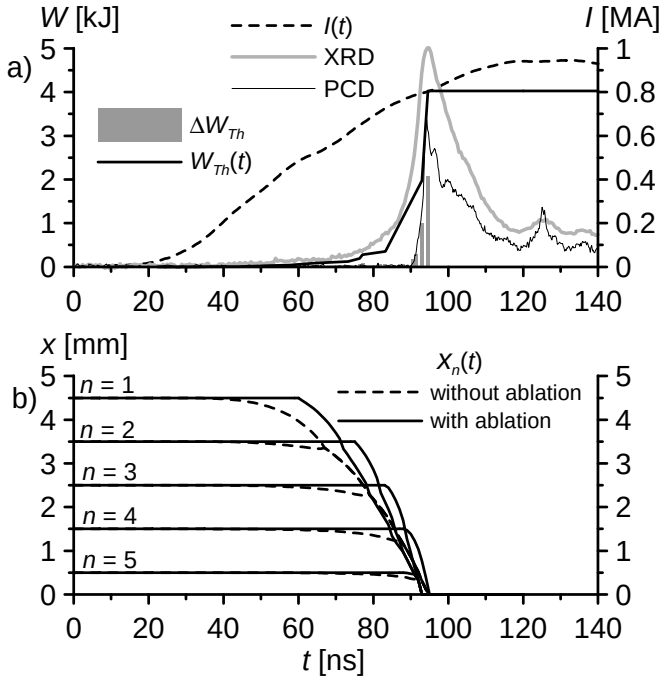

FIG. 5. (a) Zebra shot No. 490 (SPWA): experimental current pulse $I(t)$ and XRD and PCD signals (both shown in arbitrary units). The WADM calculation of thermalized kinetic energy $W_{Th}(t)$ and its instantaneous increments ΔW_{Th} (presented by the histogram). (b) Simulated trajectories of the imploding wires $x_n(t) = |\xi_n(t)|$ in this shot shown in ablation and no-ablation approximations.

IV. WADM MODELING OF PLANAR WIRE ARRAYS

One of the intrinsic features of planar wire array geometries is an uneven current partition through the array wires, which often results in a cascade-type implosion of a wire array [18, 19]. In its turn, the implosion character depends on the planar array geometry. Below in this section we shall consider single planar wire array (SPWA) and double planar wire array (DPWA), built of a single wire row [8, 9] and two wire rows [11] respectively.

Two Zebra shots No. 490 and No. 487 will be considered in particular. The composition of the loads in this shots (Al wires) facilitates the comparison of these shot with the Cobra shot No. 658 considered above in order to understand the effects due to array geometry. Besides, the dynamics of both Zebra shots No. 490 and 487 has been analyzed earlier in no-ablation approximation with the WDM simulations [19]. In the WADM simulations we shall use the same value of the ablation rate coefficient for the Al wires $G = 7$ μg/mm$\cdot$(ns^{-1}MA^{-2}) as in the Cobra shot No. 658.

A. Single planar wire array

Fig. 5 presents the experimental data and the WADM calculations for the Zebra shot No. 490. In planar array configuration the wire ablation time is now different for each wire. Yet, the parameter f_i [Eq. (33)] still can be used if we replace t_{0D} with the implosion time t_{nab} calculated in no-ablation approximation

$$f_i = \frac{t_{imp}}{t_{nab}} \ . \tag{51}$$

The WADM simulation yields $t_{imp} = t_{nab} = 95$ ns, so that $f_i = 1$. The array implosion corresponds to the sharp rise of the PCD signal in Fig. 5(a).

Implosion trajectories in Fig. 5(b) are calculated in ablation and no-ablation approximations. The difference between these two approximations somehow resembles the one shown in Fig. 1 for a cylindrical array that is reproduced for 5 separate contours. However, the implosion dynamics picture in planar geometry is even more complex, since all wires of planar array are inductively and dynamically coupled.

Two-dimensional distributions of plasma mass density $\rho(x, y)$ and the axial component of the electric current density $j_z(x, y)$, reconstructed from the WADM simulation data according to Eq. (21) are shown in Fig. 6. Due to the mutual inductance [18, 19], the outermost array wires conduct the major part of the electric current and, thus, ablate with significantly higher rate. Once these outermost wires are completely ablated while all remaining plasma is swept toward the array center, the electric current switches to the adjacent

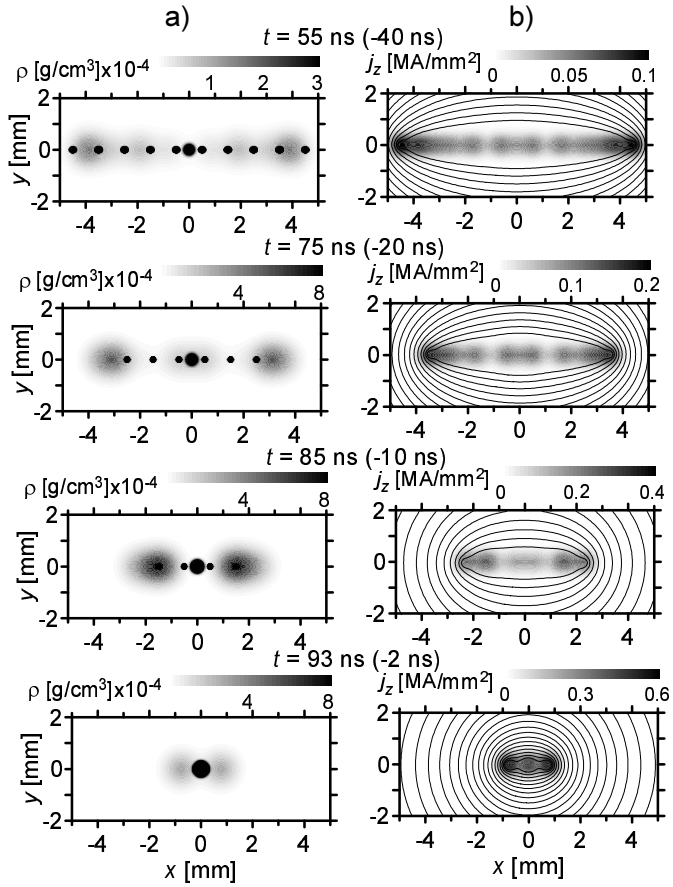

FIG. 6. Two-dimensional distributions of the plasma mass density ρ (a) and the current density j_z (b) on the complex plane (x, y) reconstructed from the WADM simulations of Zebra shot No. 490 (SPWA) and shown for four different times. The global magnetic field lines are also shown in plot (b). Time in the round brackets referred to the array implosion.

inner wires. This process repeats itself resulting in cascade-type ablation of the array wires, which is coupled with the cascade-type array implosion, considered earlier in [18, 19].

B. Double planar wire array

Below we shall consider an implosion of the double planar wire array load in Zebra shot No. 487. The experimental current and x-ray pulses are presented in Fig. 7, while two-dimensional distributions of plasma mass density and the axial component of the electric current density are given at four different moments in Fig. 8.

The load implosion times obtained by the WADM for Zebra shot No. 487 in ablation and no-ablation approximations are represented by quite close numbers: $t_{nab} = 92$ ns and $t_{imp} = 95$ ns, so that $f_i = 1.03$. In no-ablation approximation the implosion of DPWA load can be represented by two competitive processes: individual implosion of each wire plane and convergence of these wire planes toward the array center [19]. However, consideration of wire ablation dynamics significantly modifies this picture.

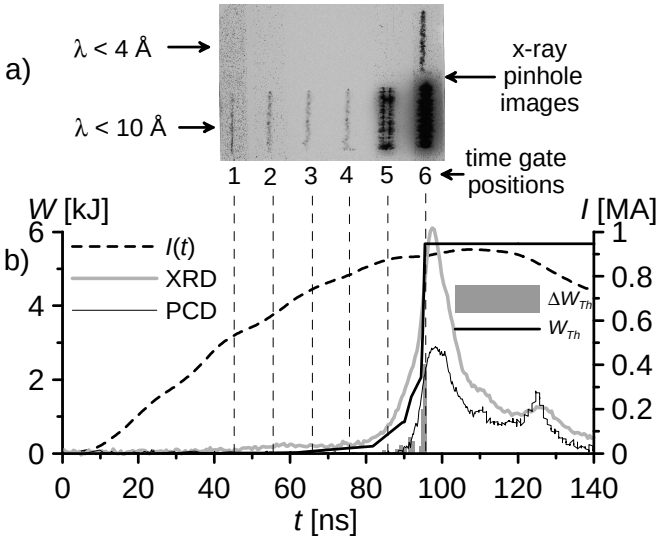

FIG. 7. Zebra shot No. 487 (DPWA): (a) time gated pinhole x-ray images recorded by six MCP frames in two spectral bands with different wavelength λ margins; and (b) experimental current pulse $I(t)$ and XRD and PCD signals (both shown in arbitrary units) with the WADM calculation of thermalized kinetic energy $W_{Th}(t)$ and its instantaneous increments ΔW_{Th} (presented by the histogram).

As we can see from Fig. 8 in a double planar geometry the load implosion dynamics features partially resemble the ones in single cylindrical and single planar configurations. In double planar geometry each wire plane ablates in a cascade-type manner, just as a single planar array, yet the ablated plasma is swept out from the wire planes in the direction toward the array center, which resembles ablation dynamics of a single cylindrical array. First, the flows of the ablated plasma from the left and right halves of each wire plane merge in front of the centers of wire planes. Then, two resultant jets of the ablated plasma move toward each other along y-axis and merge at the geometrical center of the load.

These characteristic features of the dynamics of ablated plasma flows predetermine multi-step precursor formation in double planar array geometry (more aspects of this discussion can be found in Refs. [11] and [26]). These characteristic features also make WADM simulations of such load quite different from the WDM simulations performed in no-ablation approximation [19] contrary to the case of a single planar geometry considered above. In particular, the multi-step precursor formation in double planar array geometry manifests in the formation of a double column structure, which can be observed in Fig. 7(a) 10 ns before the load implosion (the line of observation of the x-ray pinhole camera for this shot is parallel to the x-axis).

The evolution of the thermalized kinetic energy $W_{Th}(t)$ calculated by the WADM for Zebra shot No. 487 is shown in Fig. 7(b). The smoothed shape of the thermalization rate $P^*(t)$, which is calculated according to Eq. (27), is compared

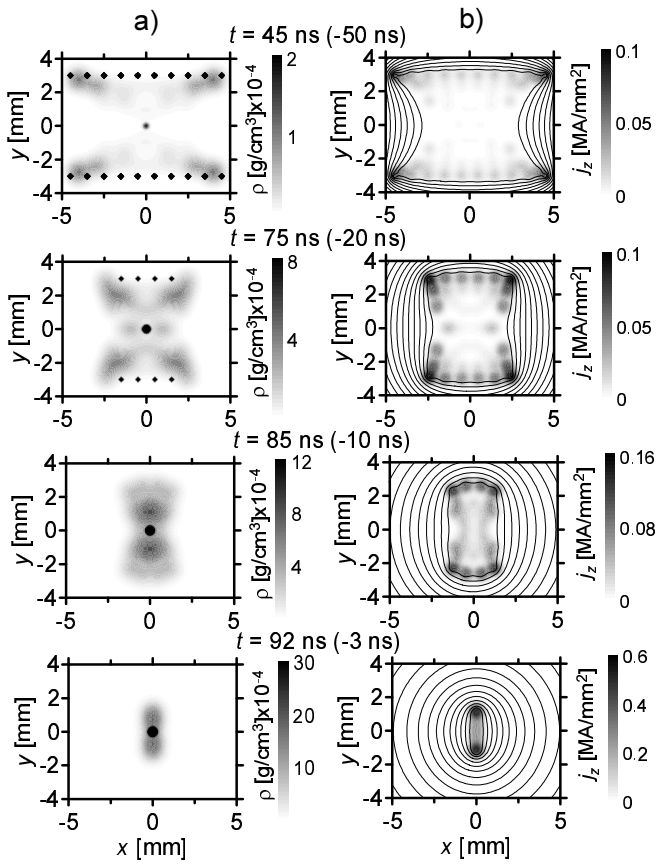

FIG. 8. Two-dimensional distributions of the plasma mass density ρ (a) and the current density j_z (b) on the complex plane (x, y) reconstructed from the WADM simulations of Zebra shot No. 487 (DPWA) and shown for four different times. The global magnetic field lines are also shown in plot (b). Time in the round brackets referred to the array implosion.

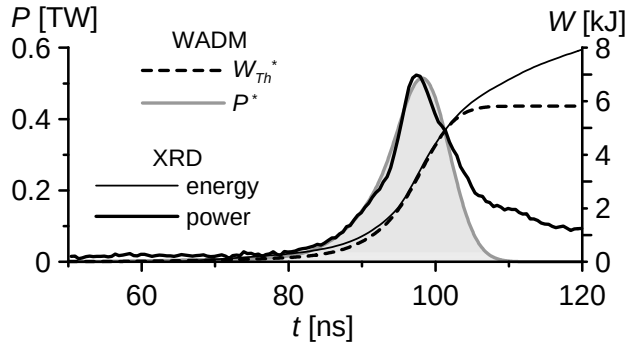

FIG. 9. Smoothed shapes of the thermalized kinetic energy W^*_{Th} and thermalization rate P^* calculated according to Eq. (27) for Zebra shot No. 487 and compared with normalized XRD signal for this shot.

TABLE II. Implosion parameters for Al wire array loads of the different geometries: compact cylindrical (CCWA), single planar (SPWA) and double planar (DPWA) wire arrays.

Shot No.	Geometry	M [μg]	t_{nab} [ns]	t_{imp} [ns]	f_i	ε_p [keV]	T^*_p [eV]	f_W
658 (Cobra)	CCWA	68	83	98	1.18	5.4	190	2.8
490 (Zebra)	SPWA	95	95	95	1	6.7	210	1.9
487 (Zebra)	DPWA	85	92	95	1.03	6.3	200	3.2

with the experimental x-ray pulse in Fig. 9. As we can see, this shape is fairly described approximately until the maximum of the x-ray burst.

As it was extensively discussed in Refs. [8–11] both sub-keV and total radiated energies are $\sim 3-5$ times higher then the calculated kinetic energy of the imploding load. Some new unconventional mechanisms of plasma heating has been proposed, such as the anomalous plasma heating (see, for example, Refs. [36, 37]). This anomalous heating mechanism is likely to be fully engaged during the stagnation phase, when the induced electric field reaches peak intensity [19, 31].

In the meantime, plasma heating at pre-stagnation and early stagnation stages is mostly defined by the thermalization of the kinetic energy, which can be fairly described by the WADM for any wire array load of arbitrary geometry. The latter feature is very useful for the design and optimization of wire array loads with the x-ray radiation pulse shaping capability [15].

C. Comparison of cylindrical and planar wire arrays

Now we shall compare the wire ablation and implosion dynamics in different wire array configurations. Our discussion will extend to the single cylindrical, single planar and double planar Al wire loads. The evolutions of the key parameters, such as the accumulated mass at the array center $M(t)$ [Eq. (37)], kinetic energy per one ion thermalized at the array center $\varepsilon(t)$ [Eq. (40)], and the current through the filament at the array center I_p, for these loads are calculated by the WADM and are shown in Fig. 10.

As we can see from the data presented in Fig. 10, the general features of the wire ablation dynamics in single and double planar array geometries resemble the ones in cylindrical array geometry discussed in the previous section of this paper. Although, one can see some differences due to specific array geometry. Due to the cascade-type wire ablation and multi-step precursor formation in single and double planar configurations we can see a bit slower mass accretion at the array center in these configurations. The same features also predetermine slightly lower values of thermalized kinetic energies per one ion ε at the central regions of these planar array configurations. In open magnetic SPWA configuration [25] the relative value of the electric current through the filament at the array center elevates up to $\sim 8\%$, which is noticeably higher than the usual value $\leq 1\%$ in cylindrical configurations.

The summaries of wire ablation dynamic parameters for different configurations of Al wire arrays are given in the

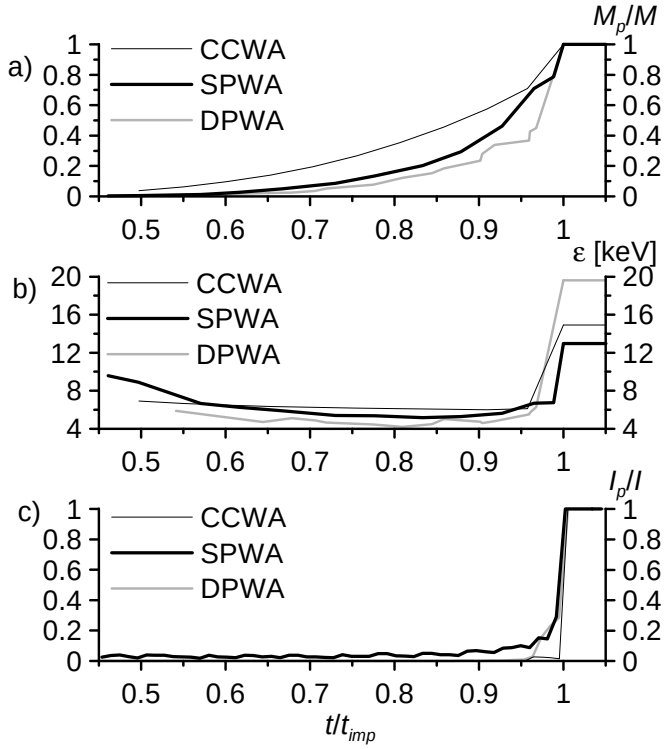

FIG. 10. Parameters of the ablation and implosion dynamics calculated by the WADM for Al wire array loads in the Cobra shot No. 658 (CCWA) and Zebra shots No. 490 (SPWA) and No. 487 (DPWA): (a) ratio of the accumulated mass at the array center M_p to the load mass M, (b) thermalized kinetic energy per one ion at the array center ε and (c) ratio of the current through the filament at the array center I_p to the load current I.

Table II. If we compare the values of parameter ε_p [Eq. 41], which is a key parameter to define the radiation features of the precursor plasma column in the correspondent radiation MHD modeling, in the Tables I and II we shall see that this value is mostly defined by the wire material, rather than load geometry.

In the meantime, the data in the Table II show that the implosion characteristics of Al wire arrays are noticeably affected by the load geometry. Despite the fact that these loads have comparable masses and sizes, the wire ablation effects are stronger for the compact cylindrical array ($f_i = 1.18$) and are weaker for the planar arrays ($f_i \approx 1$).

Using the WADM we can check the dependence of the parameter f_i on load mass M. The simulations in Fig. 11 have been performed for the three loads of the same geometries as shown in the Table II, as the masses of these loads have been varied in the range $50-150\ \mu$g. As expected, the data in this figure show a general trend of increasing ablation effects for heavier loads (in a cylindrical configuration the ablation and implosion times scale differently: $t_a \propto M$ and $t_{0D} \propto \sqrt{M}$, increasing f_τ and f_i for heavier loads).

At the same time, the specific values of the parameter f_i depend on array geometry due to the different characters of mass distribution in different load geometries. In a cylindrical array all the mass is initially located at the array

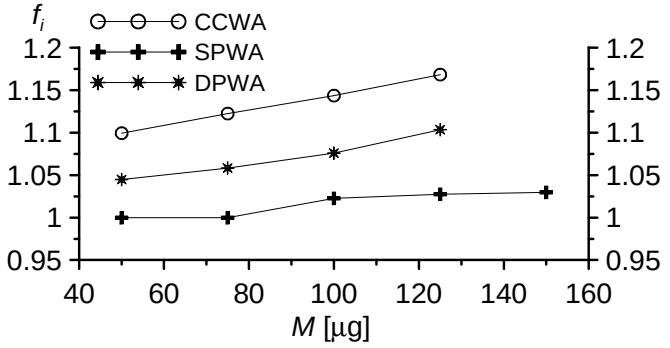

FIG. 11. Dependence of the parameter f_i [Eq. (33)] on the load mass M for compact cylindrical (CCWA), single planar (SPWA) and double planar (DPWA) wire arrays according to the WADM.

periphery and has to imploded toward the array center. In single planar geometry the mass is equally distributed along the implosion trajectories of the peripheral wires, decreasing the value of the "effective mass" to implode. Double planar array can be considered as a "hybrid" configuration, which combines the above features from both cylindrical and single planar configurations.

With the increase of the current pulse amplitude, assuming that the current rise time stays the same, in order to keep the same load implosion time one has to increase the load mass M proportionally to the square of current amplitude $M \propto I^2_{max}$ [see, for example, Eqs. (1)–(2)]. With $\alpha = 2$ in Eq. (8) the wire ablation rate should scale exactly in the same way $dM/dt \propto I^2_{\max}$. Thus, we should not observe any difference in current scaling trends for CCWA, SPWA and DPWA configurations at the facilities with stiff current pulse. This statement is corroborated by the WADM simulations.

In the meantime, at the major multi-MA wire array facilities the actual current pulse shape is defined by the load inductance as well as by the rate of the load inductance change (consider, for example, the Saturn facility [13, 14] at SNL). The dynamics of load inductance change is quite different in cylindrical and planar load geometries, mainly due to the cascade-type load implosion in the latter case. As a result, in the experiments at 5 MA Saturn generator [14] quite heavy CCWA loads have to be designed in order to match the desired implosion times with SPWA loads. That fact was used as a possible explanation of a much lower x-ray power and yield current scaling for CCWA loads as compared to the SPWA loads [14]. The similar trends for current scaling of the x-ray radiation power and yield for CCWA and SPWA loads have been reported in the experiments at enhanced current (up to 1.4 MA) at Zebra facility [38].

V. CONCLUSION

The Wire Ablation Dynamics Model is able to describes in a single simulation two separate processes of the wire ablation and array implosion in arbitrary load geometry and

wire material composition. Since a typical WADM simulation is a few hundred times faster than the adequate MHD simulation, the WADM is a perfect tool suited for wire array load design and optimization in wide parameter range.

The analysis of experimental data reveals that even at the same current the rate of the wire mass ablation depends on the wire material. The WADM accounts for this feature by attributing the specific value of wire ablation rate coefficient to each wire material. Comparative WADM simulations of the loads of different geometries at different generators with the once determined ablation rate coefficients demonstrate an excellent consistency with experimental data.

Among three wire materials discussed in this paper, the aluminum was found to have the fastest ablation rate, while the copper has the slowest ablation rate and the stainless steel has the moderately slow one. The WADM shows that the slower wire ablation results in higher ablation velocity, higher kinetic energy of the ablated plasma flow, and more significant delay of heavy load implosion due to the ablation effects, which manifest the most in a cylindrical array configuration and almost vanish in a single planar array configuration.

The current distribution inside the wire array load is given by the WADM using the approximation of the inductive current partition and is calculated simultaneously with the momentum redistribution between the ablating array wires and the inward streams of the ablated plasmas. However, the WADM does not provide the details of current distribution inside the core-corona structure of the ablating wire. Hence, some specific cases involving initially heterogeneous wire structures such as, for example, wires coated with a small amount of hydrocarbons from the imperfect vacuum, should be treated differently, for example, applying the time-varying ablation rate coefficients.

Among the most important applications of the WADM one can emphasize the design and modeling of the wire array loads with specific properties for the Inertial Confinement Fusion research and laboratory astrophysics experiments. The WADM simulations can also be used to facilitate the radiation MHD modeling of wire array plasmas.

ACKNOWLEDGMENTS

The authors thank D.A. Hammer and his research team for the support of experimental campaign at Cornell University and Nevada Terawatt Facility personnel for help with experiments at UNR. The authors greatly appreciate numerous productive discussions with P. Sasorov, S. Lebedev, B. Jones, C. Coverdale, K. Struve, A. Chuvatin and L. Rudakov. This work was supported by the NNSA under the DOE Cooperative Agreements DE-FC52-06NA27588 and DE-FC52-06NA27586.

[1] R. B. Spielman, C. Deeney, G. A. Chandler *et al.*, Phys. Plasmas **5**, 2105 (1998).
[2] C. Deeney, M. R. Douglas, R. B. Spielman *et al.*, Phys. Rev. Lett. **81**, 4883 (1998).
[3] M. E. Cuneo, R. A. Vesey, J. L. Porter *et al.*, Phys. Plasmas **8**, 2257 (2001).
[4] R. A. Vesey, M. C. Herrmann, R. W. Lemke *et al.*, Phys. Plasmas **14**, 056302 (2007).
[5] B. Jones, D. J. Ampleford, R. A. Vesey *et al.*, Phys. Rev. Letters **104**, 125001 (2010).
[6] S. V. Lebedev, F. N. Beg, S. N. Bland *et al.*, Phys. Plasmas **8**, 3734 (2001).
[7] S. V. Lebedev, F. N. Beg, S. N. Bland, J. P. Chittenden, A. E. Dangor, and M. G. Haines, Phys. Plasmas **9**, 2293 (2002).
[8] V. L. Kantsyrev, L. I. Rudakov, A. S. Safronova *et al.*, IEEE Trans. Plasma Sci. **34**, 2295 (2006).
[9] V. L. Kantsyrev, A. S. Safronova, D. A. Fedin *et al.*, IEEE Trans. Plasma Sci. **34**, 194 (2006).
[10] V. L. Kantsyrev, L. I. Rudakov, A. S. Safronova *et al.*, High Energy Density Physics **3**, 136 (2007).
[11] V. L. Kantsyrev, L. I. Rudakov, A. S. Safronova *et al.*, Phys. Plasmas **15**, 030704 (2008).
[12] A. S. Safronova, V. L. Kantsyrev, A. A. Esaulov *et al.*, Phys. Plasmas **15**, 033302 (2008).
[13] B. Jones, M. E. Cuneo, D. J. Ampleford *et al.*, Sandia Report SAND2007-6337. Office of Scientific and Technical Information of the U.S. Department of Energy (www.osti.gov), document No. 920806 (2007).
[14] B. Jones, M. E. Cuneo, D. J. Ampleford *et al.*, Sandia Report SAND2008-6166. Office of Scientific and Technical Information of the U.S. Department of Energy (www.osti.gov), document No. 941403 (2008).
[15] V. L. Kantsyrev, A. S. Safronova, A. A. Esaulov *et al.*, Journal of Physics: Conference Series **244**, 032030 (2010).
[16] A. S. Safronova, V. L. Kantsyrev, A. A. Esaulov *et al.*, Journal of Physics: Conference Series **244**, 032031 (2010).
[17] V. L. Kantsyrev, A. A. Esaulov, A. S. Safronova *et al.*, Phys. Rev. E **84**, 046408 (2011).
[18] A. A. Esaulov, A. L. Velikovich, V. L. Kantsyrev, T. A. Mehlhorn, and M. E. Cuneo, Phys. Plasmas **13**, 120701 (2006).
[19] A. A. Esaulov, V. L. Kantsyrev, A. S. Safronova, A. L. Velikovich, M. E. Cuneo, B. M. Jones, K. W. Struve, T. A. Mehlhorn, Phys. Plasmas **15**, 052703 (2008).
[20] E. P. Yu, B. V. Oliver, D. B. Sinars, T. A. Mehlhorn, M. E. Cuneo, P. V. Sasorov, M. G. Haines, S. V. Lebedev, Phys. Plasmas **14**, 022705 (2007).
[21] E. P. Yu, M. E. Cuneo, M. P. Desjarlais *et al.*, Phys. Plasmas **15**, 056301 (2008).
[22] A. L. Velikovich, I. V. Sokolov, and A. A. Esaulov, Phys. Plasmas **9**, 1366 (2002).
[23] A. A. Esaulov, V. L. Kantsyrev, A. S. Safronova *et al.*, HEDP **5**, 166 (2009).
[24] K. M. Williamson, V. L. Kantsyrev, A. A. Esaulov *et al.*, Phys. Plasmas **16**, 012704 (2009).
[25] V. L. Kantsyrev, A. S. Safronova, A. A. Esaulov *et al.*, HEDP **5**, 115 (2009).

[26] K. M. Williamson, V. L. Kantsyrev, A. A. Esaulov *et al.*, Phys. Plasmas **17**, 112705 (2010).
[27] V. V. Alexandrov, I. N. Frolov, M. V. Fedulov *et al.*, IEEE Trans. Plasma Sci. **30**, 559 (2002).
[28] P. V. Sasorov, B. V. Oliver, E. P. Yu, and T. A. Mehlhorn, Phys. Plasmas **15**, 022702 (2008).
[29] M. E. Cuneo, E. M. Waisman, S. V. Lebedev *et al.*, Phys. Rev. E **71**, 046406 (2005).
[30] M. E. Cuneo, D. B. Sinars, E. M. Waisman *et al.*, Phys. Plasmas **13**, 056318 (2006).
[31] A. Esaulov, Phys. Plasmas **13**, 042506 (2006).
[32] D. L. Peterson, R. L. Bowers, K. D. McLenithan *et al.*, Phys. Plasmas **5**, 3302 (1998).
[33] D. L. Peterson, R. L. Bowers, W. Matuska *et al.*, Phys. Plasmas **6**, 2178 (1999).
[34] A. A. Esaulov, B. S. Bauer, V. Makhin *et al.*, Phys. Rev. E **77**, 036404 (2008).
[35] C. A. Coverdale, A. S. Safronova, V. L. Kantsyrev *et al.*, Phys. Rev. Letters **102**, 155006 (2009).
[36] P. V. Sasorov, Sov. J. Plasma Phys. **18**, 143 (1992).
[37] A. A. Esaulov and P. V. Sasorov, Plasma Phys. Rep. **23**, 576 (1997).
[38] K. M. Williamson, V. L. Kantsyrev, A. S. Safronova *et al.*, AIP Conference Proceedings **1088**, American Institute of Physics, 141 (2009).